Computer Assisted Mechanics and Engineering Sciences, 15: 37–44, 2008.

A hybrid atomistic-continuum finite element modelling of nanoindentation and experimental verification for copper crystal

Paweł Dłużewski, Marcin Maździarz, Grzegorz Jurczak
Interdisciplinary Centre for Materials Modelling
Institute of Fundamental Technological Research, PAS, Warsaw, Poland

Piotr Traczykowski
Institute of Plasma Physics and Laser Microfusion, Warsaw, Poland

Koichi Niihara
Extreme Energy-Density Research Institute, Nagaoka University of Technology, Nagaoka, Japan

Roman Nowak
Nordic Hysitron Laboratory, Helsinki University of Technology, Helsinki, Finland

Krzysztof Kurzydłowski
Interdisciplinary Centre for Materials Modelling
Faculty of Materials Science and Engineering, Warsaw University of Technology, Warsaw, Poland

(Received April 10, 2007)

Problem of locally disordered atomic structure is solved by using a hybrid formulation in which nonlinear elastic finite elements are linked with discrete atomic interaction elements. The continuum approach uses nonlinear hyperelasticity based upon the generalized strain while the atomistic approach employs the Tight-Binding Second-Moment Approximation potential to create new type of elements. The molecular interactions yielding from constitutive models of TB-SMA were turned into interactions between nodes to solve a boundary value problem by means of finite element solver. In this paper we present a novel way of modelling materials behaviour where both discrete (molecular dynamics) and continuum (nonlinear finite element) methods are used. As an example, the nanoindentation of a copper sample is modelled numerically by applying a hybrid formulation. Here, the central area of the sample subject to nanoindentation process is discretised by an atomic net where the remaining area of the sample far from indenters tip is discretised by the use of a nonlinear finite element mesh.

1. Introduction

In recent years the numerical modelling of large atomic systems has been performed using methods based on molecular dynamics; see for example [5, 11, 15, 19, 22, 23]. In these calculations the system is typically composed of many millions of atoms. For larger and more complicated problems the number of freedom degrees in the system dramatically increases and one quickly becomes inhibited by time-constraints affordable for a practical computation. In such cases, for millions of variables, it is convenient to assume a different approach based on methods of continuum mechanics. The

champion of which is finite element analysis; see for example [7, 10, 14]. In finite element analysis one is less hindered by the scale of the system.

The most important and common difference obtained by comparing solutions of atomic and continuum methods appears at points where forces acting on the particles induce significant rearrangement of the underlying lattice structure. Physical phenomena incited by large excursions of the atoms from their initial position in perfect crystal, have been studied and modelled using a combination of atomistic and continuum methods; for example, crack propagation [2, 17], stress wave propagation [20], mechanical dynamics of defects and interfaces [27], dislocation emission at the heterostructure interface [1, 3] and stress-strain distributions in nanostructures [12, 18]. In cases cited above, combined atomistic continuum simulations are limited to two-dimensional models or, at the most, to quasi three-dimensional models with periodicity along one coordinate. From both, the theoretical and practical point-of-view a combination of atomistic and continuum methods seems to be a natural way forward for modelling large systems. In this way, the crystalline structure close to dislocation core is modelled with discrete molecular dynamics, while continuum mechanics aptly deals with motions of the structure far from dislocations. Thus, in this article we take full advantage of the both formalisms by considering a hybrid formulation where atomistic and continuum parts coexist on an equal footing.

This article is organised as follows. In Section 2, we give an overview of used numerical techniques, in particular, on the specific form of the potential governing atomic dynamics and principles of nonlinear finite element calculations. Following this, in Section 3, we present and discuss our results for hybrid atomistic-continuum modelling. Finally, in Section 4, we draw conclusions and summarise.

2. Hybrid atomistic-continuum finite element modelling

To simulate the indentation process of nanocrystalline copper we have performed a hybrid molecular-continuum calculation. In this way we combine discretisation at the atomic level near the indenters tip and simulation of the surrounding region with a finite element mesh (as illustrated in Fig. 1). As sketched above, both elastic and plastic deformations take part in the dynamics during the nanoindentation process. In particular, plastic deformation appears as a result of the rearrangement of the crystal structure on an atomic level and this should be taken into account in modelling the indentation process. This phenomenon is taken into account here by performing a regeneration of the list of atomic interactions at each step of the nanoindentation.

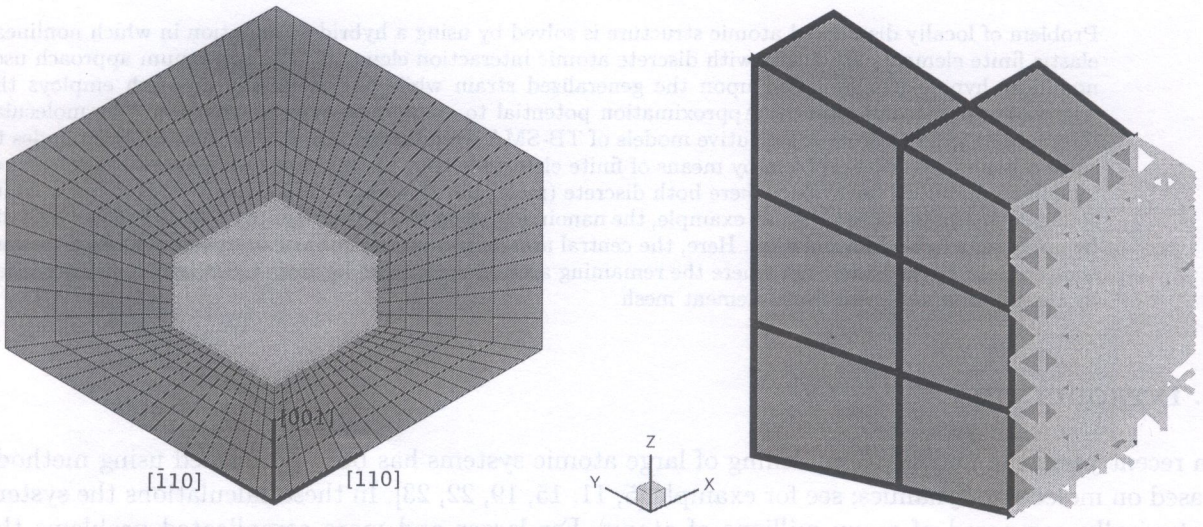

Fig. 1. The initial state of the fractional system with molecular and continuum parts (on the left) and a zoom of the interface between atomistic and continuum regions (on the right). Here, red blocks denote continuum finite elements, while green lines denote atomic interaction elements.

In our simulation the indenter is given by a rigid body with a spherical tip of radius 10 nm. Impressed atoms 'stick' to its surface during the indentation process. Pure elastic behaviour of the crystal far from the indenters tip was simulated by the use of 27-node Lagrangian hyper-elastic brick elements. The crystallographic orientation was chosen to be [110][−110]; see Fig. 1. This orientation assures ideal conformity between discrete positions of atoms and nodes of the continuum mesh on the interface. The sample was assumed to reside on a rigid base while the side-faces remain unconstrained. This approach allows for the correct dynamics of the system as a whole and in particular, allows for compression and/or extension of the system in the xy-plane. Furthermore, due to the four-point rotational symmetry of problem, only a fractional (quarter) part of the sample was calculated (as in Fig. 1) after applying a proper boundary conditions in the planes of symmetry. The bottom of sample is fully fixed, outer planes possess periodic boundary condition and inner planes of symmetry are constrained in normal direction.

The dimension of the calculated sample was arbitrarily chosen to be $40 \times 40 \times 12.5$ nm, while the atomistic region covers a volume $15 \times 15 \times 4.5$ nm within the finite element mesh. The atomic part of the system was composed of $N \sim \mathcal{O}(10^4)$ atoms of copper, the interactions of which were modelled by a Tight-Binding Second-Moment-Approximation (TB-SMA) potential. In our calculation we assumed copper to be face-centred-cubic structure with the conventional lattice parameter $a = 3.6151$ Å.

2.1. TB-SMA molecular potential

It is recognised that empirically based many-body potentials can reproduce well the structural properties of most metals. A relatively simple scheme for taking into account the electronic and structural properties based on a small set of adjustable parameters, is the Tight-Binding Second-Moment-Approximation (TB-SMA) potential [4].

The total cohesive energy of the system (see Fig. 2) is given by

$$E_c = \sum_i \left(E_R^i + E_B^i\right) , \tag{1}$$

where the Born-Mayer ion-ion repulsion term E_R^i and 'hopping' term E_B^i are summed over all atomic positions $i, j \in \{1, \ldots, N\}$, and defined by

$$E_i^{(R)} = \sum_j A e^{-p\left(\frac{r_{ij}}{r_0}-1\right)} \tag{2}$$

$$E_i^{(B)} = -\sqrt{\sum_j \xi^2 e^{-2q\left(\frac{r_{ij}}{r_0}-1\right)}} . \tag{3}$$

where r_0 is the nearest neighbor distance and r_{ij} is current distance between atoms. The free parameters A, ξ, p and q are fitted to data determined from experiment and, for crystalline copper investigated here, we assumed the values [4]: $A = 0.0855$ eV, $\xi = 1.224$ eV, $p = 10.960$ and $q = 2.278$. The inter-atomic forces are

$$f_n^i = -\frac{\partial E_i}{\partial r_i} . \tag{4}$$

In terms of finite element method the molecular interactions can be treated as two-node 'pseudo-elements', so-called because there is no shape function for TB-SMA elements, in contrast to traditional bar finite elements. On the pseudo-element mesh, each node represents a single atom. By calculating forces between nodes (atoms) we are able to find configuration of a point at which the molecular region is in self- equilibrium. Constructing the model in this manner allows one type of element (TB-SMA) to be connected with a different type of element (continuum) in a relatively straight-forward way as illustrated in Fig. 1b. A more detailed description is presented in [5].

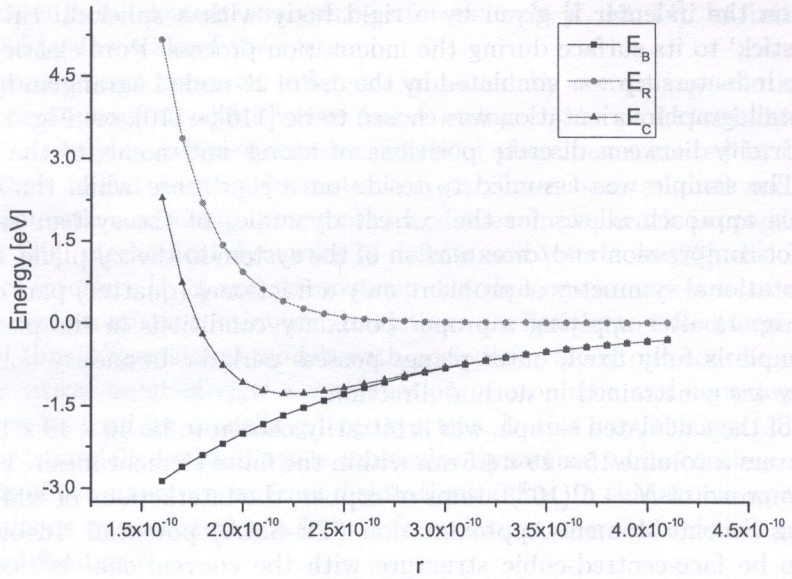

Fig. 2. Cohesive, repulsive and band energy

2.2. Nonlinear hyper-elastic finite elements

Anisotropic hyper-elastic models compose a very narrow group among numerous continuum models describing elastic behaviour of a material. Let us emphasise that the most familiar *anisotropic* hyperelastic models, such as the St. Venant–Kirchhoff and the Biot models, change strongly their instantaneous stiffness under large deformation. Moreover, the stiffness evolution often significantly differs from the behaviour of real materials. Neglecting anomalous behaviour, we can expect that with respect to molecular effects *the instantaneous stiffness of crystalline solids increases under compression and decreases under extension.* This nonlinear elastic effect is responsible for many phenomena observed experimentally. For instance, due to the different stress-strain response during the extension and compression we can observe that around an edge dislocation the volume expansion of the crystal lattice occurs, see [8, 21]. The asymmetry in the elastic stress-strain response is demonstrated also in the form of negative values of third-order elastic constants measured experimentally for many crystals, see [24–26]. Thus, applying elastic constitutive models which behave just conversely (*i.e.* St. Venant–Kirchhoff or Biot model) can be the cause of many undesirable effects such as improper proportion between stress values, sizes of extended and compressed regions or even erroneous negative volume expansion induced by interaction of dislocations in elastic continuum. Therefore, the use of a new elastic and elastic-plastic constitutive models whose behaviour could be more adjusted to the nonlinear behaviour of real crystal structures, is indispensable.

According to the polar decomposition theorem, the deformation gradient $\mathbf{F}$ can be decomposed into the orthogonal rotation tensor $\mathbf{R}$ and the right or left stretch tensor, $\mathbf{U}$ or $\mathbf{V}$, respectively, $\mathbf{F} = \mathbf{RU} = \mathbf{VR}$. The Lagrangian ($\widehat{\boldsymbol{\varepsilon}}$) and Eulerian ($\boldsymbol{\varepsilon}$) logarithmic strain tensors can be defined by means of the following isotropic functions,

$$\widehat{\boldsymbol{\varepsilon}} \stackrel{\text{df}}{=} \ln u_i \, \mathbf{u}_i \otimes \mathbf{u}_i \,, \tag{5}$$

$$\boldsymbol{\varepsilon} \stackrel{\text{df}}{=} \ln v_i \, \mathbf{v}_i \otimes \mathbf{v}_i \,, \tag{6}$$

where u_i , $\mathbf{u}_i$, v_i , $\mathbf{v}_i$ denote respectively i-th eigenvalues and eigenvectors of the right and left stretch tensors. It can be proved that to balance the energy for an arbitrarily chosen deformation process the Cauchy stress has to be governed by the following equation, see [6],

$$\boldsymbol{\sigma} = \mathbf{R} \left(\widehat{\boldsymbol{\mathcal{A}}} : \widehat{\rho} \frac{\partial \psi}{\partial \widehat{\boldsymbol{\varepsilon}}} \right) \mathbf{R}^T \det \mathbf{F}^{-1}, \tag{7}$$

where the fourth-order tensor $\widehat{\mathcal{A}}$ decomposed in the vector basis $\{\mathbf{u}_i\}$ composed of eigenvectors of the right stretch tensor is represented by the following non-vanishing components

$$\widehat{\mathcal{A}}_{ijij} = \widehat{\mathcal{A}}_{ijji} = \begin{cases} \delta_{ij}\, u_i\; f'(u_i) & \text{for } u_i = u_j\,, \\ \frac{u_i u_j [f(u_i) - f(u_j)]}{u_i^2 - u_j^2} & \text{for } u_i \neq u_j\,, \end{cases} \tag{8}$$

where $\widehat{\rho} = \rho \det \mathbf{F}$, $f'(u_i) = \frac{\mathrm{d}f(u)}{\mathrm{d}u}|_{u=u_i}$, see [16]. Let us consider the hyper-elastic material governed by the following constitutive equation stated for the specific strain energy

$$\psi = \frac{1}{2\widehat{\rho}}\, \widehat{\boldsymbol{\varepsilon}} : \widehat{\mathbf{c}} : \widehat{\boldsymbol{\varepsilon}}, \tag{9}$$

where $\widehat{\mathbf{c}}$ is the fourth-order tensor of elastic stiffness. Substitution Eq. (9) into (7) leads to

$$\boldsymbol{\sigma} = \mathbf{R}\left(\widehat{\mathcal{A}} : \widehat{\mathbf{c}} : \widehat{\boldsymbol{\varepsilon}}\right) \mathbf{R}^T \det \mathbf{F}^{-1}. \tag{10}$$

This constitutive model based on the generalised strain measure takes into account the most of the well-known anisotropic elastic models.

Our finite element (FE) algorithm is based on the integration of the equilibrium equation, which can be equivalently rewritten in relation to the current and/or reference configuration. Writing this equation in current configuration we find the following local form,

$$\mathrm{div}\boldsymbol{\sigma} = \mathbf{0}, \tag{11}$$

where the Cauchy stress is a nonlinear function of the displacement vector $\mathbf{a}$ and its gradient $\nabla\mathbf{a}$. Applying the virtual work principle we find the following nonlinear matrix equation,

$$\mathbf{P}(\mathbf{a}) = \mathbf{f}\,, \tag{12}$$

where

$$\mathbf{P} = \int_v \nabla^T \mathbf{W}\boldsymbol{\sigma}\, \mathrm{d}v, \tag{13}$$

$$\mathbf{f} = \int_{\partial v} \mathbf{W}\boldsymbol{\sigma}\, \mathrm{d}\mathbf{s}. \tag{14}$$

$\mathbf{W}$ denotes here the weighting function determined in relation to the current (wanted) configuration. In the interior of finite elements the distribution of displacement field is governed by the relation

$$\mathbf{a}(\mathbf{x}) = \sum_{i=1,27} N_i^u(\mathbf{x})\, \mathbf{a}_i\,, \tag{15}$$

where N_i^u and $\mathbf{a}_i$ denote the second-order Lagrangian shape function spanned on 27 nodes of 3D brick element and the nodal displacements, respectively.

3. Results and discussion

The simulation was divided into small displacement steps. The indentation depth D is given by finite steps $\Delta D = 1.5\,\text{Å}$ of the indenter tip into the sample. Compared to crystallographic distance between nearest copper atoms equal 2.55 Å, this choice of ΔD makes it possible to take into account gradual changes in atomic interactions. The authors performed a test comparing the results of $\Delta D = 5 \times 0.3\,\text{Å}$ and $\Delta D = 1.5\,\text{Å}$ for a few first steps of the algorithm, the results were exactly the same. After applying proper values of vertical displacement to atoms interacting with the indenter, the problem reduces to the solution of a boundary-value problem. Our results are shown in Figs. 3–5.

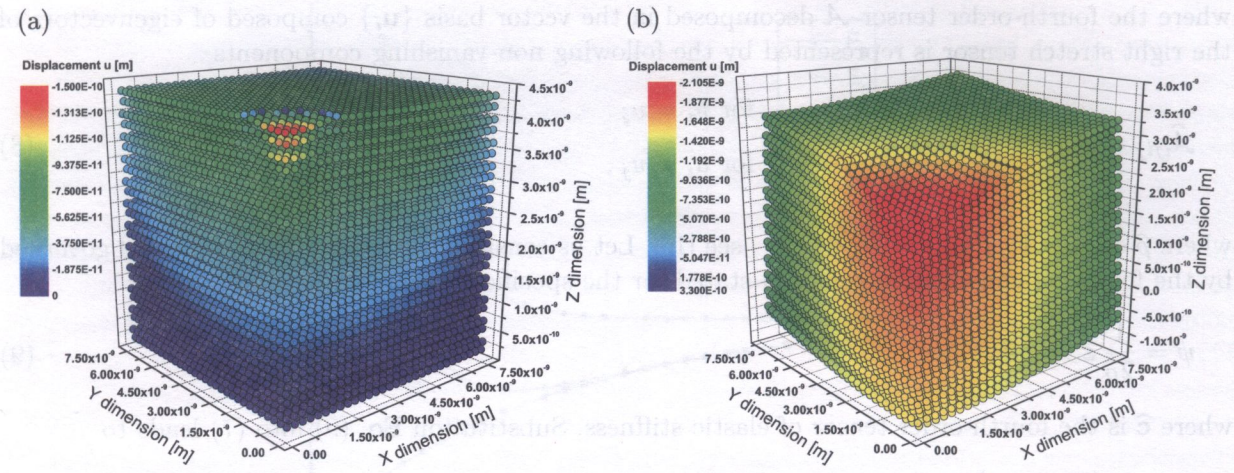

Fig. 3. Molecular region after indentation depths of (a) 1.5 Å and (b) 21.0 Å

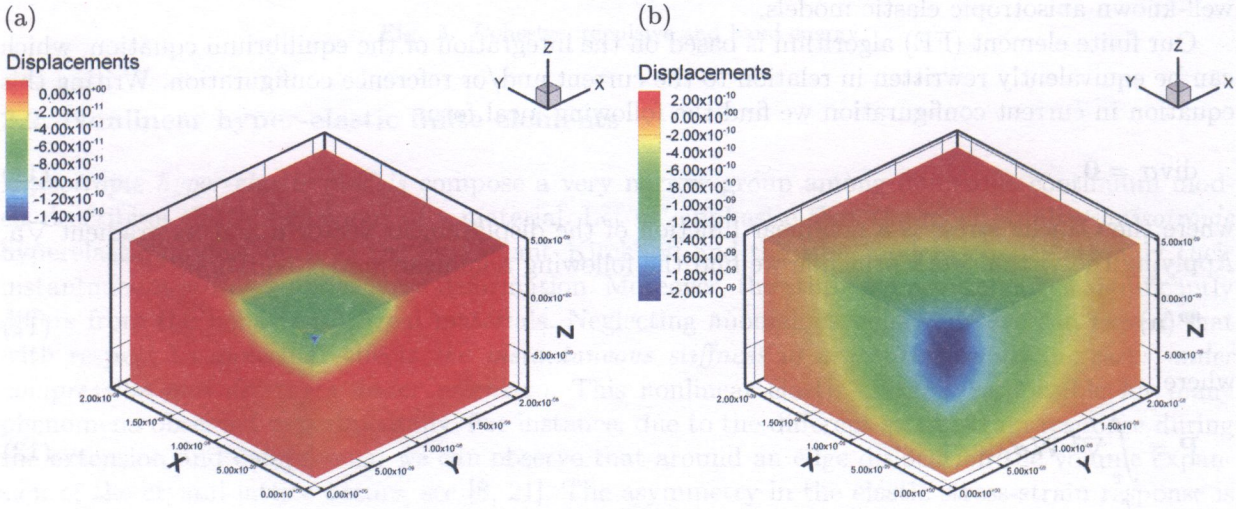

Fig. 4. Hybrid finite element atomic mesh after indentation depth (a) 1.5 Å, (b) 21.0 Å– vertical displacement

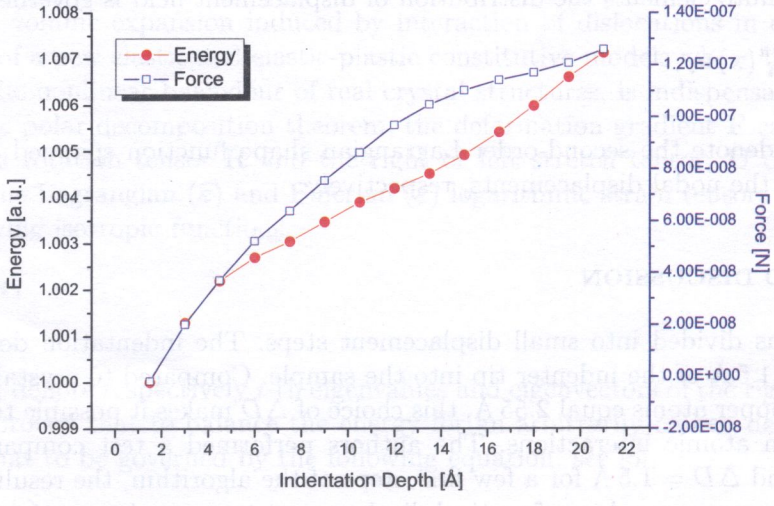

Fig. 5. Energy of atomic area and force acting on indenter vs. depth of indenter tip

From mechanical point of view, simulation of indentation process can be divided into two main stages. The first part of the nanoindentation runs until the indenter reaches a depth $4.5-6.0$ Å and terminates at the first sign of reorganisation of the atomic bonds. Until this depth the structure worked wholly elastically and force-depth curve seems to be linear, however its derivative suggest small instantaneous stiffness drop. The second part of the simulation describes plastic deformation of copper crystal. During this part the plastic rearrangement of the crystal structure starts and it is revealed in the energy of the system as a deviation from the linear relation energy-depth, see Fig. 5. During this stage of deformation, because of reorganisation of the atomic bonds, dislocations propagate through the molecular region and shift molecular bonds. Rearrangement of the molecular mesh at each step of the indentation causes a rapid energy change and produces further dislocation.

Finally, we comment that following depth $D \geq 12$ Å, relative to the sample's thickness an indentation process exceeds the prescribed 10% rule [9], and loaded system undergoes complete plastic deformation leading to an approximate flat force-indentation curve, typical for pure plastic materials. However near depth $D \geq 18$ Å one can observe plastic hardening.

4. Conclusions

In this article we have presented the results of an atomistic-continuum finite element modelling of a nanoindentation process on copper sample. Many conclusion yields from these simulation, among others

- By employing a hybrid framework we were able to model elastic and elastic-plastic processes and use atomic discretisation for this part of the system where atomic effects are important, while the remaining part of the system was filled by nonlinear finite element mesh.

- Some difficulties can arise from a possible mismatch in conformity between the natural configurations of both structure. In other words, the position of FE nodes situated on the atomic-continuum border must take the position of atoms to connect with atomic net. This limits the application of the present method to special crystallographic planes of perfect lattice. Otherwise, in the case of use the non-conformal FE-MD meshes a transient region in which the atomic mesh overlaps with the finite element one must be applied.

- There are other reasons why the transient regions are often used in many calculations. For example, when the nonlinear elastic characteristics of the continuous and atomistic nets differ significantly under loading then some stress concentration manifesting in deformation discontinuity under loading is observed between the atomistic and FE meshes. To avoid this problem the transient region is helpful. In our previous works we tested how the instantaneous stiffness changes under loading for various nonlinear elastic continuum and molecular models [5]. On the basis of this experience and the present simulation we conclude that in this particular case of applying the TB-SMA model together with hyperelastic anisotropic Hooke's law based on the logarithmic strain measure such concentrations of stress are not observed. This is because the stiffness of the two parts changes very similarly in the domain of large elastic deformation.

- In the future applications of hybrid FE-MD boundary zone should be automated by use of computer preprocessors adopted to generate simultaneously the complementary parts of the molecular and continuum meshes. This will be a new enterprise for preprocessors available mainly for FE method coinciding here with the use of a molecular net.

Acknowledgments

This work has been supported by the Ministry of Science and Higher Education, Projects COST/200/2006, 3 T08A 021 29, and by the European Commission, Project MRTN-CT-2004-005583. This research was also partially supported by the Academy of Finland (Research Consortium NAKAMA and NANOTOMO).

References

[1] M.E. Bachlechner, A. Omeltchenko, A. Nakano, R.K. Kalia, P. Vashishta, I. Ebbsjo, A. Madhukar. Dislocation emission at the silicon/silicon nitride interface: A million atom molecular dynamics simulation on parallel computers. *Phys. Rev. Lett.*, **84**: 322, 2000.

[2] J.Q. Broughton, F.F. Abraham, N. Berstern, E. Kaxiras. Concurrent coupling of length scales: Methodology and application. *Phys. Rev. B*, **60**: 2391–2403, 1999.

[3] D. Chrobak, K. Nordlund and R. Nowak. Non-dislocation origin of GaAs nanoindentation pop-in event. *Phys. Rev. Lett.*, **98**: 045502, 2007.

[4] F. Cleri, V. Rosato. Tight-binding potentials for transition metals and alloys. *Phys. Rev. B*, **48**: 22–33, 1993.

[5] P. Dłużewski, P. Traczykowski. Numerical simulation of atomic positions in quantum dot by means of molecular statics. *Archives of Mechanics*, **55**: 501–515, 2003.

[6] P. Dłużewski. Anisotropic hyperelasticity based upon general strain measure. *Computational Material Science*, **29**: 379, 2004.

[7] P. Dłużewski, G. Maciejewski, G. Jurczak, S. Kret, J.-Y. Laval. Nonlinear FE analysis of residual stresses induced by dislocations in heterostructures. *J. Elasticity*, **60**: 119–129, 2000.

[8] M.J. Horodon, B.L. Averbach. Precision density measurements on deformed copper and aluminum single crystals. *Acta Metallurgica*, **9**: 247, 1961.

[9] Y.R. Jeng, C.M. Tan. Theoretical study of dislocation emission around a nanoindentation using a static atomistic model. *Phys. Rev. B*, **69**: 104109, 2004.

[10] G. Jurczak, G. Maciejewski, S. Kret, P. Dłużewski, P. Ruterana. Modelling of indium rich clusters in MOCVD InGaN/GaN multilayers. *Journal of Alloys and Compounds*, **382**: 10–16, 2004.

[11] J. Knap, M. Ortiz. An analysis of the quasicontinuum method. *J. Mech. Phys. Solids*, **49**: 1899–1923, 2001.

[12] E. Lidorikis, M.E. Bachlechner, R.K. Kalia, A. Nakano, P. Vashishta, G.Z. Voyiadjis. Coupling length scales for multiscale atomistic-continuum simulations: Atomistically-induced stress distributions in Si/Si_3N_4 nanopixels. *Phys. Rev. Lett.*, **87**: 086104, 2001.

[13] Y. Liu, B. Wang, M. Yoshino, S. Roy, H. Lu, R. Komanduri. Combined Numerical Simulation and Nanoindentation for Determining Mechanical Properties of Single Crystal Copper at Mesoscale. *J. Mech. Phys. Solids*, **53**: 2718-2741, 2005.

[14] R. Nowak, T. Manninen, K. Heiskanen, T. Sekino, A. Hikasa, K. Niihara, T. Takagi. Peculiar surface deformation of sapphire: Numerical simulation of nanoindentation. *Appl. Phys. Lett.*, **83**: 5214–5216, 2003.

[15] R. Nowak, F. Yoshida, D. Chrobak, K.J. Kurzydlowski, T. Takagi, T. Sasaki. Nanoindentation examination of crystalline solid surfaces in *Encyclopedia of Nanoscience and Nanotechnology*. Am. Sci. Publ. ed. S.H. Nalwa, 2008, in press.

[16] R.W. Ogden. *Non-linear Elastic Deformations*. Ellis Horwood, Chichester, 1984.

[17] H. Rafii-Tabar, L. Hua, M. Gross. A multi-scale atomistic-continuum modelling of crack propagation in a two-dimensional macroscopic plate. *J. Phys. Condens. Matter*, **10**: 2375–2387, 1998.

[18] V.B. Shenoy, R. Miller, E.B. Tadmor, R. Phillips, M. Ortiz. Quasicontinuum models of interfacial structure and deformation. *Phys. Rev. Lett.*, **80**: 742–745, 1998.

[19] V.B. Shenoy, R. Miller, E.B. Tadmor, D. Rodney, R. Phillips, M. Ortiz. An adaptive finite element approach to atomic-scale mechanics — the quasicontinuum method. *J. Mech. Phys. Solids*, **47**: 611–642, 1999.

[20] A. Smirnowa, L.V. Zhigilei, B.J. Garrison. A combined molecular dynamics and finite element method technique applied to laser induced pressure wave propagation. *Comput. Phys. Commun.*, **118**: 11–16, 1999.

[21] F. Spaepen. Interfaces and stresses in thin films. *Acta Materialia*, **48**: 31, 2000.

[22] E.B. Tadmor, R. Philips, M. Ortiz. Mixed atomistic and continuum models of deformation in solids. *Langmuir*, **12**: 4529–4534, 1996.

[23] E.B. Tadmor, M. Ortiz, R. Philips. Quasicontinuum analysis of defects in solids. *Phil. Mag. A*, **73**: 1529, 1996.

[24] C. Teodosiu. *Elastic Models of Crystal Defects*. Springer-Verlag and Editura Academiei, Berlin–Bucureşti, 1982.

[25] S.N. Vaidya, G.C. Kennedy. Compressibility of 18 elemental solids to 45 kb. *J. Phys. Chem. Solids*, **31**: 2329–2345, 1970.

[26] S.N. Vaidya, G.C. Kennedy. Compressibility of 22 elemental solids to 45 kb. *J. Phys. Chem. Solids*, **33**: 1377–1389, 1972.

[27] E. Weinan, Z. Huang. A dynamic atomistic-continuum method for the simulation of crystalline materials. *J. Comput. Phys.*, **182**: 234–261, 2002.